Astron. Astrophys. 355, 1080–1086 (2000)

ASTRONOMY AND ASTROPHYSICS

Magnetic field geometries of two slowly rotating Ap/Bp stars: HD 12288 and HD 14437

G.A. Wade[1], **D. Kudryavtsev**[2], **I.I. Romanyuk**[2], **J.D. Landstreet**[3], **and G. Mathys**[4]

[1] Astronomy Department, The University of Toronto at Mississauga, Mississauga, Ontario, Canada L5L 1C6
[2] Special Astrophysical Observatory, Russian Academy of Sciences, 357 147 Niznij Arkhyz, Russia
[3] Physics & Astronomy Department, University of Western Ontario, London, Ontario, Canada N6A 3K7
[4] European Southern Observatory, Casilla 19001, Santiago 19, Chile

Received 20 December 1999 / Accepted 20 January 2000

Abstract. In this paper we report magnetic field models and basic physical parameters for the slowly rotating Ap/Bp stars HD 12288 and HD 14437.

Using new and previously published mean longitudinal magnetic field, mean magnetic field modulus, and HIPPARCOS photometric measurements, we have inferred the rotational periods of both stars (HD 12288: $P_{\rm rot} = 34\overset{\rm d}{.}9 \pm 0\overset{\rm d}{.}2$; HD 14437: $P_{\rm rot} = 26\overset{\rm d}{.}87 \pm 0\overset{\rm d}{.}02$). From the magnetic measurements we have determined the best-fit decentred magnetic dipole configurations. For HD 12288, we find that the field geometry is consistent with a centred dipole, while for HD 14437 a large decentring parameter ($a = 0.23\ R_*$) is inferred. Both stars show one angle in the ambiguous (i, β) couplet which is smaller than about 20°. This is consistent with the observation of Landstreet & Mathys (2000), who point out that almost all magnetic Ap stars with periods longer than about 30 days exhibit magnetic fields aligned with their rotational axis.

Key words: polarization – stars: chemically peculiar – stars: evolution – stars: individual: HD 12288 – stars: individual: HD 14437 – stars: magnetic fields

1. Introduction

A significant fraction of all A-type and late B-type stars have strong, globally ordered magnetic fields. However, models of the surface magnetic field configuration exist for only a handful of these objects. Because these magnetic fields convey information about the formation and pre-main sequence history of these stars (e.g. Moss 1989), offer a means to probe the structure and dynamics of the stellar interior (e.g. Moss 1990), and strongly influence other important physical processes occurring in the stellar envelope (e.g. Babel & Michaud 1991; Babel 1992; Landstreet et al. 1998), a much broader understanding of their magnetic characteristics is required. In this paper, as part of a continuing programme aimed at constructing magnetic field models for stars throughout the F0-B2 temperature range, we report magnetic field geometry models and basic physical properties of two stars: the A2p CrSi star HD 12288 and the B9p CrEuSi star HD 14437.

Magnetically split lines were first observed in the spectrum of the A2p CrSi star HD 12288 (=BD+68 144=HIP 9604; $V = 7.75$) by Preston (1971). Mathys et al. (1997) obtained 20 measurements of the mean magnetic field modulus $B_{\rm s}$ (also known as the surface field) of this star within the context of a broad survey of magnetic fields in sharp lined Ap stars. They also discovered that this object is a spectroscopic binary (SB1), with a radial velocity amplitude of at least 16 km s^{-1} and an orbital period of at least 4 years. Leroy (1995) noted a strong interstellar polarisation toward this star, and was unable to measure the broadband linear polarisation variation. Both the trigonometric parallax and photometric variation of HD 12288 were obtained by the HIPPARCOS satellite.

Magnetically split lines were reported in the spectrum of the B9p CrEuSi star HD 14437 (=BD+42 502=HIP 10951; $V = 7.26$) by Mathys et al. (1993). Mathys et al. (1997) reported 17 measurements of $B_{\rm s}$, but were unable to determine a unique rotational period. The trigonometric parallax and photometric variation of HD 14437 were also obtained by the HIPPARCOS satellite.

2. Observations

2.1. Longitudinal magnetic field measurements

The longitudinal magnetic field represents the disc-integrated line-of-sight component of the magnetic field. Observations of the longitudinal fields of HD 12288 and HD 14437 were obtained at the Special Astrophysical Observatory of the Russian Academy of Sciences (SAO) and at the University of Western Ontario Elginfield Observatory (UWO).

2.1.1. SAO measurements

Thirteen longitudinal field measurements of HD 12288 and 28 measurements of HD 14437 were obtained at the SAO, using the 6 metre telescope and main stellar spectrograph equipped with an achromatic circular polarisation analyser. SAO mag-

Send offprint requests to: G.A. Wade

netic data obtained before JD 2445901 were recorded on Kodak IIaO photographic plates, with a reciprocal linear dispersion of 9 Å/mm. Those obtained after JD 2450000 were measured from CCD spectra, recorded using the spectroscopic CCD with a reciprocal linear dispersion of 14 Å/mm. The longitudinal field was inferred from measurements of the relative displacement of spectral lines in the left and right circular polarisation spectra. Quoted uncertainties are at the 1σ level, and were computed from the distribution of the displacement measurements. The SAO equipment and observing technique are described by Glagolevski et al. (1986) and Borisenko et al. (1991).

In addition to the spectropolarimetric measurements, two measurements of HD 14437 obtained on JD 2449555 and 2449556 were acquired using the SAO photoelectric Balmer line magnetometer. This instrument is similar in principle to the UWO photoelectric polarimeter described below.

2.1.2. UWO measurements

Seven longitudinal field measurements of HD 12288 and 6 measurements of HD 14437 were obtained at UWO. The UWO photoelectric polarimeter was used as a Balmer line Zeeman analyser at the UWO 1.2 metre telescope. The polarimeter measures the fractional circular polarisation in the wings of Hβ, isolated using narrowband interference filters, at ± 5.0 Å from line centre. It has been shown (Landstreet 1982) that the polarisation thus measured is linearly related to the mean longitudinal magnetic field. For these observations, mean conversion factors $\gamma = 12400$ G and $\gamma = 13200$ G per percent circular polarisation were found respectively for HD 12288 and HD 14437 from Hβ line scans. Uncertainties associated with the UWO measurements were determined from photon counting statistics, and are at the 1σ level. A more detailed description of the instrument and observing technique is given by Landstreet (1980).

As will become apparent, the different measurement techniques described above can result in systematic differences between the longitudinal field as measured using metallic lines (denoted $\langle H_z \rangle$) and that measured using Balmer lines (denoted B_ℓ). We will retain these different symbols to help reinforce that the two methods do in fact measure somewhat different quantities, and we should therefore not expect them to be fully consistent.

2.2. Mean magnetic field modulus measurements

Respectively 28 and 32 spectroscopic observations of HD 12288 and HD 14437 were obtained by Mathys et al. (1997) and Mathys et al. (1999) in the context of a larger study of magnetic fields in Ap stars. From these spectra measurements of the mean magnetic field modulus $B_{\rm s}$ were obtained. The field modulus, which represents the disc integrated strength of the magnetic field, was inferred from fits to the magnetically split components of the Fe II $\lambda 6149.2$ Zeeman doublet. The relevant observing, reduction and analysis procedures are described in detail by Mathys et al. (1997).

For HD 12288 the mean value of $B_{\rm s}$ is 7978 G, with a minimum measured value of 7439 G and a maximum value of 8496 G, while for HD 14437 the mean value of is 7665 G, with a minimum measured value of 7024 G and a maximum value of 8219 G. For HD 14437 Mathys et al. (1997) estimate the uncertainty of individual measurements to be about 200 G. While Mathys et al. do not estimate the uncertainty of individual measurements for HD 12288, they do provide the rms deviations (120 G) about the best-fit curve. We provisionally adopt this value as the 1σ uncertainty of individual measurements.

2.3. HIPPARCOS *photometry*

Respectively 164 and 100 photometric measurements of HD 12288 and HD 14437 were obtained in the context of the HIPPARCOS mission, in the HIPPARCOS photometric system described in Volume 1 of The HIPPARCOS and Tycho Catalogues (ESA 1997). The measured magnitude (in the HIPPARCOS photometric system) of HD 12288 is 7.779 with an rms scatter of 0.016 mag, while that of HD 14437 is 7.258 with an rms scatter of 0.013 mag. The photometry is available in Volume 17 of the HIPPARCOS Catalogue, CD-ROM no. 3 (ESA 1997). In the following analysis a single spurious observation of HD 14437 (obtained on JD 2448844.510) and two spurious observations of HD 12288 (obtained on JD 2448024.534 and JD 2448313.639) have been removed.

3. Rotational periods

3.1. HD 12288

Lomb-Scargle periodograms (Press & Rybicki 1989) of each of the 3 datasets were computed in the period range 1-100 days. The HIPPARCOS photometry periodogram displays a single strong peak at $35\overset{\rm d}{.}3 \pm 0\overset{\rm d}{.}6$, while the longitudinal field periodogram displays a single strong peak at $35\overset{\rm d}{.}0 \pm 0\overset{\rm d}{.}5$. This indicates that the rotational period lies within the unique range $34\overset{\rm d}{.}5 - 35\overset{\rm d}{.}9$. In the periodogram of the field modulus measurements, only one strong peak (the strongest peak in the periodogram at $34\overset{\rm d}{.}9 \pm 0\overset{\rm d}{.}2$) falls within this unique range. This period is consistent with that reported by Mathys et al. (1997) and by Wolff & Morrison (1973), and in particular rules out periods near 1 d reported by the latter authors. We have adopted the field modulus period as the rotational period of HD 12288 and phased all data according to the ephemeris:

$$\mathrm{JD} = 2448499.87 + 34\overset{\rm d}{.}9 \cdot \mathrm{E}, \qquad (1)$$

where the zero point corresponds to an epoch of field modulus maximum.

The phased data are shown in Table 1 and in Fig. 1. While the UWO data describe an approximately sinusoidal variation when phased according to the adopted ephemeris ($\chi^2/\nu = 1.0$ for a first-order Fourier fit), the SAO data do not ($\chi^2/\nu = 9.5$). A careful examination of the SAO data shows that observations obtained at similar rotational phases are consistent within their error bars, suggesting that the SAO error bars are not underestimated and that the large reduced χ^2 for a first-order fit results

Table 1. Journal of longitudinal magnetic field observations of HD 12288 obtained using the UWO photoelectric polarimeter (UWO) and the SAO Zeeman analyser (SAO). Phases are calculated from the ephemeris cited in the text and σ_B is the 1 standard deviation uncertainty.

JD-240 0000	Phase	$B_\ell \pm \sigma_B$ (G)	Observatory
49949.860	0.639	-1200 ± 520	UWO
49975.803	0.382	-320 ± 370	UWO
50257.784	0.462	-220 ± 360	UWO
50761.608	0.898	-1870 ± 500	UWO
50774.310	0.262	-896 ± 78	SAO CCD
50855.383	0.585	-846 ± 128	SAO CCD
50855.398	0.585	-880 ± 170	SAO CCD
50861.309	0.755	-1674 ± 214	SAO CCD
50861.326	0.755	-1440 ± 137	SAO CCD
51040.485	0.889	-2678 ± 92	SAO CCD
51064.384	0.573	-986 ± 90	SAO CCD
51184.132	0.005	-3090 ± 103	SAO CCD
51184.163	0.006	-3060 ± 94	SAO CCD
51239.217	0.583	-740 ± 80	SAO CCD
51253.635	0.996	-3160 ± 430	UWO
51267.651	0.398	-630 ± 560	UWO
51274.619	0.597	-530 ± 470	UWO
51452.180	0.685	-1100 ± 130	SAO CCD
51453.233	0.715	-1240 ± 120	SAO CCD
51477.374	0.407	-860 ± 100	SAO CCD

from real departures from such a variation. Indeed, if we fit the SAO data using a second-order Fourier fit, the reduced χ^2 drops to 0.8. Such departures from a pure sinusoid may well be due to abundance inhomogeneities, which would be detected in the metallic line observations, but not in the Balmer line data (as observed).

When the field modulus and photometric measurements are phased according to this ephemeris they describe approximately sinusoidal variations, with reduced χ^2s 1.3 (field modulus) and 1.2 (photometry).

3.2. HD 14437

Periodograms of each the 3 datasets have been computed in the period range 1-100 days. The periodogram of the HIPPARCOS photometry displays only one prominent peak at $26\overset{\mathrm{d}}{.}65^{+0.7}_{-0.3}$, and clearly indicates that the rotational period is within the unique range 26.35-27.35 days.

The periodogram of the field modulus measurements shows a single peak within the unique period range defined by the photometry, at $26\overset{\mathrm{d}}{.}83^{+0.2}_{-0.15}$.

The periodogram of the longitudinal field measurements shows a series of sharp peaks within the range defined by the photometric and field modulus data. The strongest of these is at $26\overset{\mathrm{d}}{.}87 \pm 0\overset{\mathrm{d}}{.}02$. The very long timespan (17.5 years) over which the longitudinal field measurements were obtained allows us to determine the rotational period very precisely. We adopt the longitudinal magnetic field period as the rotational period of HD 14437.

Table 2. Journal of longitudinal magnetic field observations of HD 14437 obtained using the SAO Zeeman analyser with photographic plates (SAO PG), the SAO Zeeman analyser with CCD (SAO CCD), the SAO Balmer line magnetometer (SAO BLM) and the UWO photoelectric polarimeter (UWO). Phases are calculated from the ephemeris cited in the text and σ_B is the 1 standard deviation uncertainty

JD-240 0000	Phase	$B_\ell \pm \sigma_B$ (G)	Observatory
44655.208	0.885	-1620 ± 255	SAO PG
44656.308	0.926	-1030 ± 255	SAO PG
44659.188	0.033	-440 ± 255	SAO PG
44660.196	0.070	-800 ± 210	SAO PG
44860.541	0.526	-2280 ± 165	SAO PG
45303.354	0.006	-1230 ± 180	SAO PG
45303.362	0.007	-1020 ± 165	SAO PG
45476.541	0.452	-2080 ± 280	SAO PG
45900.493	0.230	-2040 ± 165	SAO PG
49555.472	0.254	-1340 ± 380	SAO BLM
49556.420	0.289	-1710 ± 460	SAO BLM
50086.731	0.025	-1410 ± 570	UWO
50087.594	0.058	-1430 ± 490	UWO
50093.587	0.281	-1910 ± 320	UWO
50320.823	0.738	-2680 ± 290	UWO
50326.820	0.961	-1270 ± 260	UWO
50335.813	0.295	-2330 ± 380	UWO
50413.523	0.187	-2040 ± 450	SAO CCD
50414.125	0.210	-2310 ± 420	SAO CCD
50415.217	0.251	-2460 ± 405	SAO CCD
50415.240	0.251	-1940 ± 270	SAO CCD
50415.269	0.252	-2570 ± 270	SAO CCD
50499.196	0.376	-2650 ± 390	SAO CCD
50499.221	0.377	-2600 ± 240	SAO CCD
50500.161	0.412	-2460 ± 330	SAO CCD
50500.188	0.413	-2050 ± 375	SAO CCD
50617.507	0.779	-1820 ± 390	SAO CCD
50643.521	0.747	-1360 ± 165	SAO CCD
50705.451	0.052	-1330 ± 315	SAO CCD
50706.410	0.088	-960 ± 165	SAO CCD
50707.412	0.125	-830 ± 150	SAO CCD
50709.602	0.206	-1370 ± 165	SAO CCD
50710.432	0.237	-2110 ± 180	SAO CCD
51039.465	0.483	-2770 ± 80	SAO CCD
51040.529	0.522	-2950 ± 90	SAO CCD
51064.370	0.410	-2360 ± 120	SAO CCD

The magnetic data have therefore been phased according to the ephemeris:

$$\mathrm{JD} = 2448473.846 + 26\overset{\mathrm{d}}{.}87 \cdot \mathrm{E}, \quad (2)$$

where phase 0.0 refers to the epoch of longitudinal field maximum.

The phased data are shown in Table 2 and in Fig. 1. The longitudinal field data subsets agree reasonably well (considering the somewhat sparse phase coverage of the B_ℓ measurements), and the reduced χ^2s of the individual subsets are 0.6 for the B_ℓ measurements and 3.0 for the metallic line measurements.

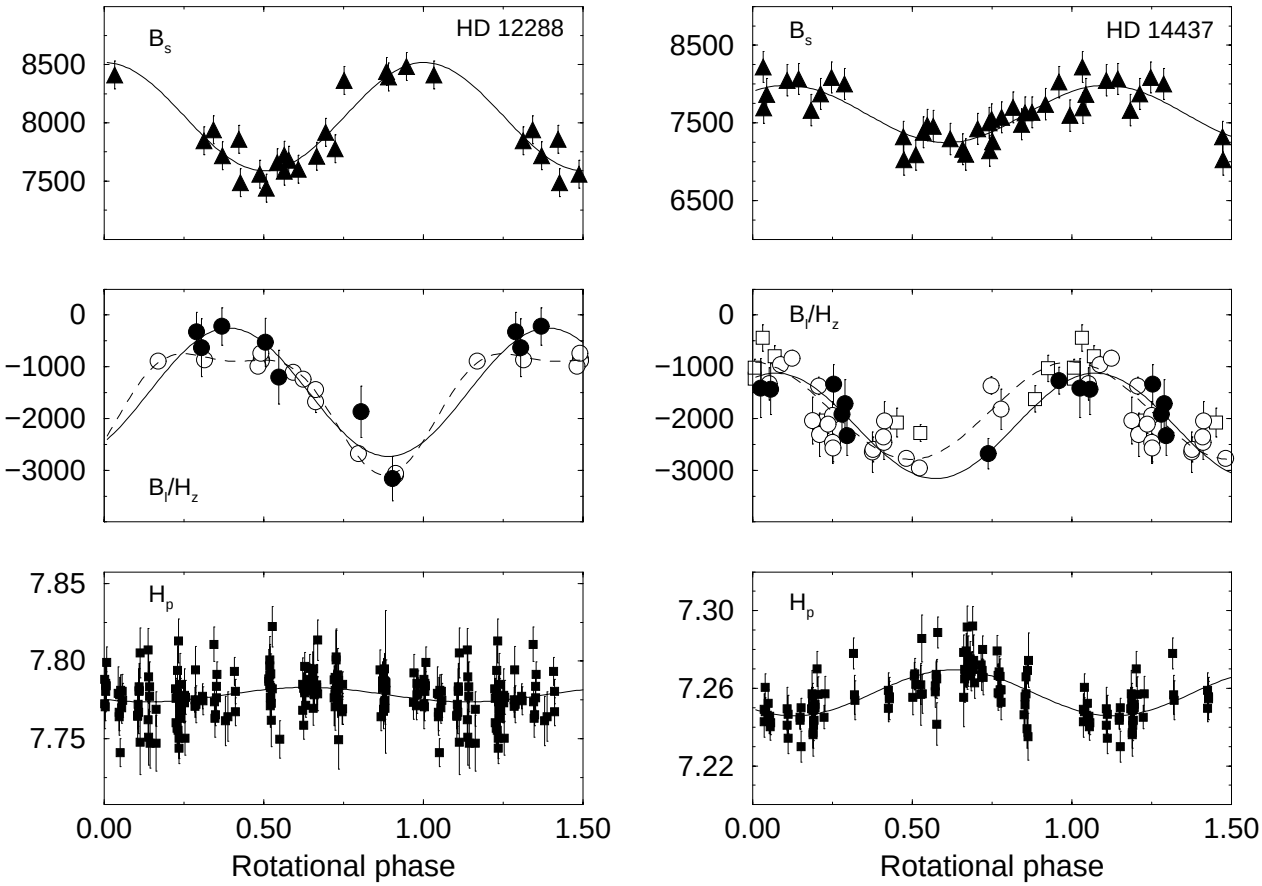

Fig. 1. Mean magnetic field modulus (in G), mean longitudinal magnetic field (in G: *Open circles* – SAO Zeeman analyser CCD measurements *Open squares* – SAO Zeeman analyser photographic plate measurements *Solid circles* – UWO/SAO Balmer line measurements), and HIPPARCOS photometry (in mag) variations of HD 12288 and HD 14437, phased according to the ephemerides described in the text. The curves are least-squares Fourier fits to the data. In the centre frames, the solid curves correspond to the B_ℓ measurements, while the dashed curves correspond to the $\langle H_z \rangle$ measurements.

All three datasets describe approximately sunusoidal variations, with reduced χ^2s of 2.5 (combined longitudinal field), 0.9 (field modulus) and 1.1 (photometry).

4. Magnetic field geometries

To determine the magnetic field configurations of HD 12288 and HD 14437 we have assumed a decentred dipole magnetic field and calculated longitudinal field and mean field modulus variations for a range of geometries. The four free parameters in the models are the inclination of the stellar rotational axis to the observer's line of sight i, the inclination of the magnetic dipole axis to the rotational axis β, the polar strength of the magnetic dipole (when centred) $B_{\rm d}$, and the decentring a of the magnetic dipole as a fraction of the stellar radius, in the direction of the magnetic axis. These four parameters are determined formally by our four independent observational constraints on the magnetic field: the (two) extrema of the average longitudinal field and the (two) extrema of the mean field modulus curve. Searching parameter space for those models consistent with the observations, we find we can describe the observed variations within their errors for the ranges of parameters shown in Table 3. An ambiguity exists between the two angular parameters i and β which is a fundamental result of such an axisymmetric magnetic field; we can identify two unique angles, but we can associate neither explicitly with the inclination i nor the obliquity β. For stars like these with small $v \sin i$ it can usually only be resolved using linear polarisation observations, although we will revisit this point in Sect. 6.

The observed and computed longitudinal field and field modulus variations of HD 12288 and HD 14437 are shown in Fig. 2.

5. Basic physical parameters

Using the trigonometric parallaxes of HD 12288 and HD 14437 obtained in the context of the HIPPARCOS mission, Gomez et al. (1998) have determined the absolute visual magnitudes of HD 12288 ($M_V = 0.5$) and HD 14437 ($M_V = 0.4$) using the so-called LM method. The uncertainties associated with these values are about ± 0.4 mag based on the parallax uncertainties reported by HIPPARCOS (ESA 1997).

The effective temperatures of these stars can be estimated from Geneva photometry (e.g. Hauck & North 1993). Us-

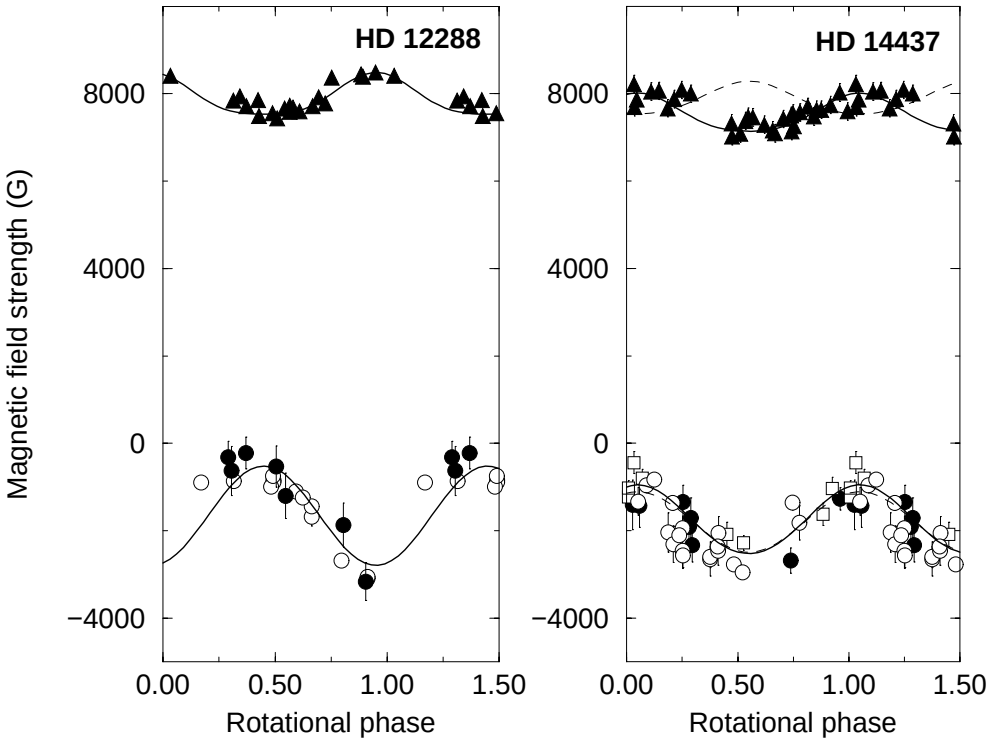

Fig. 2. Observed and computed longitudinal field and field modulus variations of HD 12288 (left frame) and HD 14437 (right frame). The solid curves are the calculations assuming the adopted models described in Table 3. The dashed curves represent the best pure dipole model achieved for HD 14437

Table 3. Adopted rotational periods and magnetic field geometries for HD 12288 and HD 14437. ϕ_+ is the phase at which the positive magnetic pole passes closest to the subsolar point

	$P_{\rm rot}$ (d)	(i,β) (°)	$B_{\rm d}$ (kG)	a	ϕ_+
HD 12288	33.9 ± 0.2	$(119 \pm 6, 21 \pm 6)$	11.8 ± 0.5	$+0.01 \pm 0.04$	0.45 ± 0.1
HD 14437	26.87 ± 0.02	$(115 \pm 6, 14^{+9}_{-4})$	$13.5^{+1}_{-0.5}$	0.23 ± 0.06	0.05 ± 0.15

ing Geneva photometric measurements published by Hauck & North (1982) we obtain $T_{\rm eff} = 8425 \pm 300$ K for HD 12288 and $T_{\rm eff} = 9285 \pm 300$ K for HD 14437. From the bolometric correction relation by Code et al. (1976) we adopt zero correction for HD 12288, and $\mathrm{BC} = -0.1$ for HD 14437. The luminosities of both stars are then given by:

$$\frac{L}{L_\odot} = 10^{-\left(\frac{M_{\rm bol} - M^\odot_{\rm bol}}{2.5}\right)}, \quad (3)$$

for $M^\odot_{\rm bol} = +4.71$ (Gray 1992). This information is sufficient to uniquely locate both stars on the H-R diagram, and they are shown along with model evolutionary tracks (Schaller et al. 1992) in Fig. 3.

From Fig. 3 we can determine the masses and ages of these objects. Furthermore, from the luminosity and effective temperature we can infer the radii, and hence the surface gravities, using the expressions:

$$\frac{R}{R_\odot} = \left(\frac{L}{L_\odot}\right)^{0.5} \cdot \left(\frac{T}{T_\odot}\right)^{-2}, \quad (4)$$

Table 4. Derived basic physical properties of HD 12288 and HD 14437

	HD 12288	HD 14437
$T_{\rm eff}$ (K)	8425 ± 300	9285 ± 300
$L/L_\odot$	48^{+24}_{-15}	58^{+26}_{-18}
$R/R_\odot$	3.3 ± 1.0	3.0 ± 0.8
$\mathcal{M}/\mathcal{M}_\odot$	2.37 ± 0.15	2.50 ± 0.15
$\log g$	3.8 ± 0.3	3.9 ± 0.3
$\log(Age)$	8.75 ± 0.07	8.60 ± 0.1

and

$$\log g = \log g_\odot + \log \frac{\mathcal{M}}{\mathcal{M}_\odot} - 2 \log \frac{R}{R_\odot}. \quad (5)$$

The basic physical properties of HD 12288 and HD 14437 are summarised in Table 4.

6. Discussion and conclusions

Both HD 12288 and HD 14437 exhibit one angle in the ambiguous (i, β) couplet which is smaller than $\sim 20°$. This is

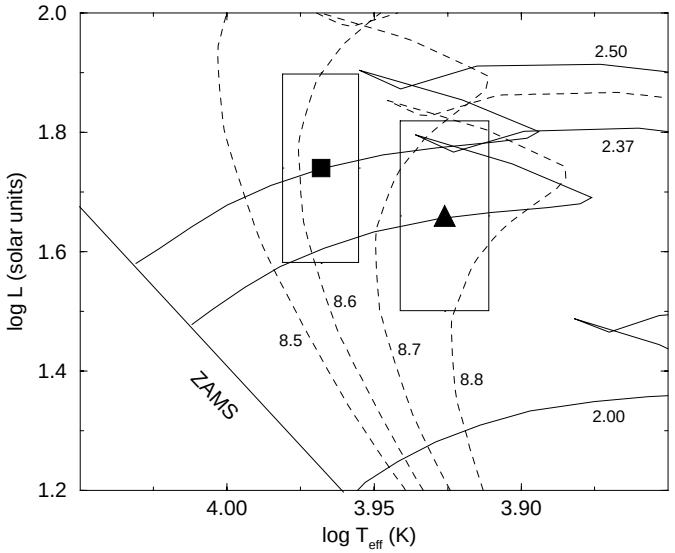

Fig. 3. H-R diagram showing the positions of HD 12288 and HD 14437. The filled square represents HD 14437 while the filled triangle represents HD 12288. Model evolutionary tracks for $\mathcal{M} = 2.0, 2.37 \text{ and } 2.5\ \mathcal{M}_\odot$ and solar metallicity are shown (Schaller et al. 1992), along with isochrones for $\log(\text{Age}) = 8.5, 8.6, 8.7 \text{ and } 8.8$ y.

consistent with the observation of Landstreet & Mathys (2000), who find, in a sample of 13 magnetic Ap stars with rotational periods longer than ~ 30 days, that 10 stars (77%) exhibit in the ambiguous couplet one angle smaller than 30°. Because inclination angles smaller than 30° are very improbable (the probability of finding $i < 30^\circ$ is only about 13.4%; Landstreet & Mathys 2000) they infer that these angles represent the magnetic obliquity β. Can we assume that this also applies for HD 12288 and HD 14437 (i.e. that the larger angles represent the inclinations of the rotational axes)? One test of this assumption is to determine whether the assumed inclination angles, when considered along with the inferred radii and rotational periods, are consistent with the observed projected rotational velocities ($v \sin i \lesssim 5$ km s^{-1}). We calculate $v \sin i$ from the expression:

$$v \sin i = \frac{50.6}{P} \frac{R}{R_\odot} \sin i, \tag{6}$$

and find $v \sin i = 4.2$ km s^{-1} for HD 12288, and $v \sin i = 5.1$ km s^{-1} for HD 14437. These values are consistent with the observational constraints, especially for HD 12288 given the report by Mathys et al. (1997) of line profile distortion due to rotational Doppler effect. Therefore the large angles in Table 3 appear to be compatible with the expected inclination angles.

Adopting therefore the argument of Landstreet & Mathys (2000), we find that our observations of HD 12288 and HD 14437 support their conclusion, namely that for stars with long rotational periods the magnetic axes are approximately aligned with their rotational axes. This is further supported by the results of Wade et al. (1997) for the slowly rotating ($P_{\rm rot} = 52\overset{\rm d}{.}0084$) Bp star HD 200311, for which a magnetic obliquity $\beta = 28^\circ$ was inferred, and by those of Wade et al. (2000) for the slowly rotating ($P_{\rm rot} = 33\overset{\rm d}{.}984$) Ap star HD 81009, for which a magnetic obliquity $\beta = 15^\circ$ is inferred. One possible interpretation of this conclusion is that the processes which led to the near total loss of rotational angular momentum in these stars also caused the alignment of their magnetic and rotational axes. We propose another possible interpretation: that the magnetic orientations of these stars are not a result of field evolution, but instead represent essentially the orientations which existed when these stars arrived on the main sequence. If those stars with nearly aligned magnetic and rotational axes lose angular momentum more efficiently than those with non-aligned axes, this would result in the observed phenomenon.

The magnetic field of HD 12288 shows only mild departures from a pure dipolar configuration; the variations are in fact consistent within the errors with a pure dipole field. In fact, HD 12288 is the only star modelled thus far using field modulus measurements for which a centred dipole is found to be consistent with the observations. HD 14437, on the other hand, exhibits variations inconsistent with those of a pure dipole. This is shown very clearly by the predictions of such a model (dashed curves in Fig. 2). This implies that the distributions of magnetic flux over the surfaces of these two stars are remarkably different, their similar values of (i, β) notwithstanding. For HD 12288 the adopted magnetic model implies a variation in field strength of about 200% over stellar surface, while for HD 14437 this variation is nearly 450%. Although it has been found (Landstreet 1988; Landstreet et al. 1989; Landstreet & Mathys 2000) that the field flux variation over the surfaces of Ap stars is usually somewhat smoother than that implied by a pure dipole or decentred dipole model, the fact remains that HD 14437 exhibits a significantly higher field strength contrast than does HD 12288.

Acknowledgements. We acknowledge the 6 metre telescope time committee for continued support of this programme. IIR and DK acknowledge the Russian Foundation for Basic Research for partial financial support. GAW acknowledges research support from J.B. Lester and C.T. Bolton. JDL acknowledges grant support from the Natural Sciences and Engineering Research Council of Canada (NSERC). This research was undertaken while GAW was an NSERC postdoctoral fellow at the University of Toronto, Department of Astronomy.

References

Babel J., 1992, A&A 258, 449
Babel J., Michaud G., 1991, ApJ 366, 560
Borisenko A.N., Markelov S.V., Ryadchenko V.P., 1991, Spec. Astrophys. Obs. Rep.
Code A.D., Bless R.C., Davis J., Brown R.H., 1976, ApJ 203, 417
ESA, 1997, ESA SP-1200, The HIPPARCOS and Tycho Catalogues. Vol. 1
Glagolevski Yu.V., Bychkov V.D., Romanyuk I.I., Chunakova N.M., 1986, Bull. Spec. Astrophys. Obs. North Caucasus 19, 26
Gomez A.E., Luri X., Gernier S., et al., 1998, A&A 336, 953
Gray D.F., 1992, The Observation and Analysis of Stellar Photospheres. Cambridge University Press
Hauck B., North P., 1982, A&A 114, 23
Hauck B., North P., 1993, A&A 269, 403
Landstreet J.D., 1980, AJ 85, 611
Landstreet J.D., 1982, ApJ 258, 639

Landstreet J.D., 1988, ApJ 326, 967
Landstreet J.D., Barker P.K., Bohlender D.A., Jewison M.S., 1989, ApJ 344, 876
Landstreet J.D., Dolez N., Vauclair S., 1998, A&A 333, 977
Landstreet J.D., Mathys G., 2000, A&A, in preparation
Leroy J.-L., 1995, A&AS 114, 79
Mathys G., Landstreet J.D., Lanz T., 1993, In: Dworetsky M.M., Castelli F., Faraggiana R. (eds.) Peculiar versus normal phenomena in A-type and related stars. IAU Colloq. 138, ASP Conference series vol. 44, p. 300
Mathys G., Hubrig S., Landstreet J.D., Lanz T., Manfroid J., 1997, A&AS 123, 353
Mathys G., Manfroid J., Wenderoth E., 1999, in preparation
Moss D., 1989, MNRAS 236, 629
Moss D., 1990, MNRAS 244, 272
Press W.H., Rybicki G.B., 1989, ApJ 338, 277
Preston G.W., 1971, ApJ 164, 309
Schaller G., Schaerer D., Meynet G., Maeder A., 1992, A&AS 96, 269
Wade G.A., Elkin V.G., Landstreet J.D., Romanyuk I.I., 1997, MNRAS 292, 748
Wade G.A., Debernardi Y., Bohlender D.A., et al., 2000, A&A, in preparation
Wolff S.C., Morrison N.D., 1973, PASP 85,141